Microporous and Mesoporous Materials 331 (2022) 111674

Contents lists available at ScienceDirect

Microporous and Mesoporous Materials

journal homepage: www.elsevier.com/locate/micromeso

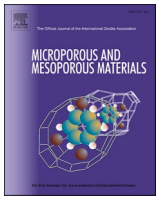

Fabrication of a novel microporous membrane based on ZIF-7 doped 1,2-bis (triethoxysilyl)ethane for H_2/CO_2 separation

Die He, Hengfei Zhang, Yi Ren, Hong Qi *

College of Chemical Engineering, Nanjing Tech University, Nanjing, 210009, China

ARTICLE INFO

Keywords:
ZIF-7 doping
Organosilica
Hydrogen
Membranes
Separation

ABSTRACT

The organosilica membranes for gas separation have been studied for approximately ten years, but the separation performance of the membranes is restricted by the trade-off effect. Therefore, the objective of this work is to design H_2-selective mixed matrix membranes by combining the good thermal stability of organosilica and remarkable H_2/CO_2 selectivity of ZIF-7. Herein, we synthesized ZIF-7 nanoparticles with an average size of 60 nm and investigated the effects of ZIF-7 doping content on the separation performance of organosilica membranes. Interestingly, it absolutely was found that with the doping content of ZIF-7 increased, H_2 permeance of ZIF-7/BTESE (1,2-bis(triethoxysilyl)ethane) membranes remained basically unchanged, whereas the permeance of larger molecular gases displayed a dramatically drop. The membrane, when the molar ratio of ZIF-7: BTESE = 0.2, showed the remarkable H_2/CO_2 (22.7) and H_2/N_2 (159) selectivity, with a comparatively outstanding H_2 permeance at 8.0×10^{-7} mol m^{-2} s^{-1}·Pa^{-1}. Our results firstly reveal that the doping of ZIFs could be strongly influenced by ZIF-7 doping contents, emphasizing the importance of doping of ZIFs for the further studies on nanoparticles-doped BTESE-derived membranes.

1. Introduction

Currently, about 80% of the world's energy consumption comes from fossil fuels. A type of non-renewable energy source, fossil fuels cause serious environmental problems after burning. Methane steam reforming and water gas shift reaction are the most common methods to produce hydrogen energy. With the advantages of greenness and sustainability, it is the most promising substitute for fossil fuels used in heat and power generation in the 21st century [1–3]. Therefore, developing more hydrogen energy technology is urgently needed for alleviating the mounting global energy and environmental crisis [4].

Compared with other technologies such as pressure swing adsorption, cryogenic distillation and solvent absorption, membrane separation technology has offered great potential for H_2/CO_2 separation, for its energy productivity, cost-effectiveness, and environmental friendliness [5,6]. Organic polymeric membranes have received wide attention with respect to low cost as well as the ease of manufacturing and processing [4,7]. However, possibly high temperature working circumstances and the potential chemical corrosion should be concerned in practical applications, which restricts the practical applications of organic polymeric membranes [8,9]. Inorganic membranes, including zeolite membranes, silica membranes, carbon-based membranes and MOF membranes [10–13]and two-dimensional membranes [14,15], are foreseen to play an important role in gas separation for H_2 and CO_2. Inorganic membranes have high thermal and chemical stability for gas separation under harsh conditions. However, successful fabrication of such membranes with high brittleness, difficult preparation, and high filling cost still remains one of the main challenges for membrane researchers. At present, a facile and efficient way to develop mixed matrix membranes (MMMs), which have become a hot research direction in gas separation, is to disperse organic/inorganic nanoparticles into polymer matrix [16]. It is hoped to synergistically combine the great separation performance of inorganic materials with the low cost of polymers to conquer their drawbacks [17–19].

Zeolite imidazolate frameworks (ZIFs) are a sub-family of metal organic frameworks (MOFs) [20], which are gaining a great deal of attention as promising fillers in MMMs due to their molecular sieving effects, good compatibility with the polymer matrix, and facile synthesis process [17,21]. Furthermore, ZIFs have attracted considerable interest because of their properties of high porosity and fascinating chemical and thermal stability [20].

Up to now, tremendous ZIF-based MMMs (ZIF-MMMs) have been

* Corresponding author.
E-mail address: hqi@njtech.edu.cn (H. Qi).

https://doi.org/10.1016/j.micromeso.2021.111674
Received 8 October 2021; Received in revised form 10 December 2021; Accepted 30 December 2021
Available online 3 January 2022

widely studied and applied in gas separation. Song et al. [22] reported the preparation of polymer matrix nano-composite membranes with good dispersion and adhesion of ZIF-8 nanoparticles within the polymer. The permeance of CO_2 on gas absorption tests were highly increased. It is clear that the loading of ZIFs prominently alters the permeability of CO_2. An early work in this field was published by Li et al. [23]. They prepared ultra-thin layers of Pebax® 1657 by doping ZIF-7 nanoparticles on PAN support via surface coating. The inclusion of ZIF-7 nanoparticles may greatly improve the separation performance for CO_2 from CH_4 and N_2. Yang et al. [24] prepared ZIF-7/PBI nano--composite membranes with the selectivity of 14.9 (H_2 permeance: 8.8 × 10^{-8} mol m^{-2} s^{-1}·Pa^{-1}) for H_2/CO_2 separation. Recently, thin MOFs-MMMs on tubular ceramic substrate modified by organosilica as bonding layer with an excellent selectivity of 53.1 (H_2 permeance: 1.094 × 10^{-8} mol m^{-2} s^{-1}·Pa^{-1}) for H_2/CO_2 separation was synthesized by Zhao et al. [18]. Kong et al. [25] synthesized MOF/organosilica (contained ZIF-8) nano-composite membranes with great gas separation performance, achieving both high selectivity of 26.5 for H_2/CH_4 and H_2 permeance of 1.06 × 10^{-6} mol m^{-2} s^{-1}·Pa^{-1} Further research that focused mainly on ZIFs doped silica membranes came into scope because tunable porosity, flexibility over substituents, and multiple chemical functionalities can be provided. In summary, it is still a huge challenge for researchers to fabricate separation membranes with both high H_2 permeance and excellent selectivity in the H_2/CO_2 separation.

In the work of the researchers mentioned above [25], the ZIF-8/organosilica membrane only showed Knudsen selectivity due to the ZIF-8 pores (0.34 nm) is very close to the kinetic diameter of CO_2 (0.33 nm). The aperture size of ZIF-7 is about 0.30 nm [23,26], just between the sizes of H_2 (0.29 nm) and CO_2 (0.33 nm), which is suitable for the development of a H_2-selective membranes [24,27–30]. The structure is shown in Fig. 1 [31,32].

Therefore, the objective of this work is to design H_2-selective mixed matrix membranes by combining the good thermal stability of organosilica and remarkable H_2/CO_2 selectivity of ZIF-7. In this work, ZIF-7 nanoparticles have been synthesized with homogeneous size distribution, and then mixed with 1,2-bis(triethoxysilyl)ethane (BTESE) sol at different ZIF-7/BTESE molar ratios (0.05,0.1,0.2). The ZIF-7/BTESE sol was coated on the tubular γ-Al_2O_3 mesoporous membranes by dip-coating, and the ZIF-7/BTESE membrane with excellent gas separation performance was successfully prepared. ZIF-7 endows the hybrid silica membranes with high permeance and selectivity because of its tunable porosity. The results of single gas permeation studies prove that both permeance and selectivity for separation of H_2/CO_2 and H_2/N_2 can be increased by the inclusion of the ZIF-7 nanoparticles compared with the BTESE membranes. We demonstrate that the resulting membranes can be promising candidates for H_2/CO_2 separation.

As far as we know, this work is the first discovery of successful silica membranes with good incorporation of ZIF-7 nanoparticles without much ZIF-7 agglomeration.

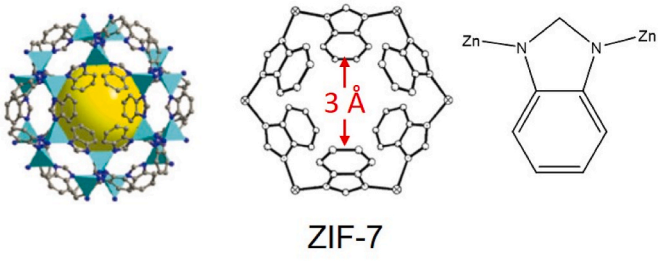

Fig. 1. 3D and chemical structure of ZIF-7 [31,32].

2. Experimental

2.1. Synthesis of ZIF-7 nanoparticles

The materials needed for the experiment can be seen in the supporting information. ZIF-7 nanoparticles were synthesized by dissolving $Zn(NO_3)_2{\cdot}6H_2O$ (590.7 mg) into methanol (50 ml) and adding DMF (50 ml) into benzimidazole (bim) (1487.5 mg) respectively. Then the Zn^{2+} source dissolved solution was quickly added into the solution containing bim while fully stirring with a magnetic bar for 6 h at room temperature. The solution was further aged at 25 °C for 12 h. After that, the mixture was separated by using a centrifuge at 8000 rpm for 5 min. Finally, the ZIF-7 nanoparticles were washed with methanol for more than 3 times and dried for 12 h at 60 °C.

2.2. Synthesis of ZIF-7/BTESE derived sols

ZIF-7/BTESE derived polymeric sols were synthesized by the following route as illustrated in Fig. 2. 0.078 g ZIF-7 nanoparticles were dissolved in 42.0 mL absolute ethanol by ultrasonic mixing, thereafter, together with 8 mL BTESE sol were mixed homogeneously with the molar ratio of 1 : 0.05 (Si: ZIF-7), where the molar ratio of ZIF-7 to BTESE (Si) was 0.05 : 1 (marked as *E*-ZIF-7-0.05). Subsequently, we tuned the molar ratios of ZIF-7 to BTESE (Si), four forms of sols were synthesized as shown below: 0 : 1 (BTESE), 0.05 : 1 (*E*-ZIF-7-0.05), 0.1 : 1 (*E*-ZIF-7-0.1) and 0.2 : 1 (*E*-ZIF-7-0.2). Synthesis of BTESE sols, fabrication of ZIF-7/BTESE membranes and related characterization can be seen in the supporting information.

2.3. Gas permeation tests

The single gas permeances (He, H_2, CO_2, N_2, CH_4, and SF_6) were used to test gas permeances performance of the as-prepared ZIF-7/BTESE membranes on a home-made device in our previous work [33]. The gas permeance was showed by the following formula:

$$P_i = \frac{F_i}{A\,\Delta P} \tag{1}$$

where P_i stands for the permeance of gas *i* (mol·m^{-2} s^{-1} Pa^{-1}), F_i is the flow rate (mol·s^{-1}), *A* and ΔP is the effective membranes area (m^2) and the transmembrane pressure (Pa), respectively.

The ideal gas separation factor (a) was showed as follows:

$$\mathrm{a} = \frac{P_i}{P_j} \tag{2}$$

where P_i is the permeance of gas *i* and P_j is the permeance of gas *j*.

3. Results and discussion

3.1. Characterization of ZIF-7 nanoparticles

The as-synthesized ZIF-7 nanoparticles were routinely characterized by various physical and chemical techniques, the results of which are provided in Fig. 3–7. The XRD pattern about the peak positions and relative intensities in Fig. 3 matches well with the simulated ZIF-7 nanoparticles and other researches on ZIF-7 [34–36], and clearly indicates that the as-synthesized particles are ZIF-7. The size of above-mentioned ZIF-7 nanoparticles displayed in the SEM pictures in Fig. 4(a) conform to the statistics obtained from Fig. 4(b), which have a uniform size distribution around 60 nm. It has been demonstrated that the selection of ZIF-7 nanoparticles size in mixed matrix membranes should be considered, including ZIF crystal form, dispersion problems, and interactions with polymer molecular chains. Abnormal sizes of ZIF-7 may cause crystal structure defects and agglomeration is likely or more serious interface incompatibility may occur. Thus, the particle size of 60

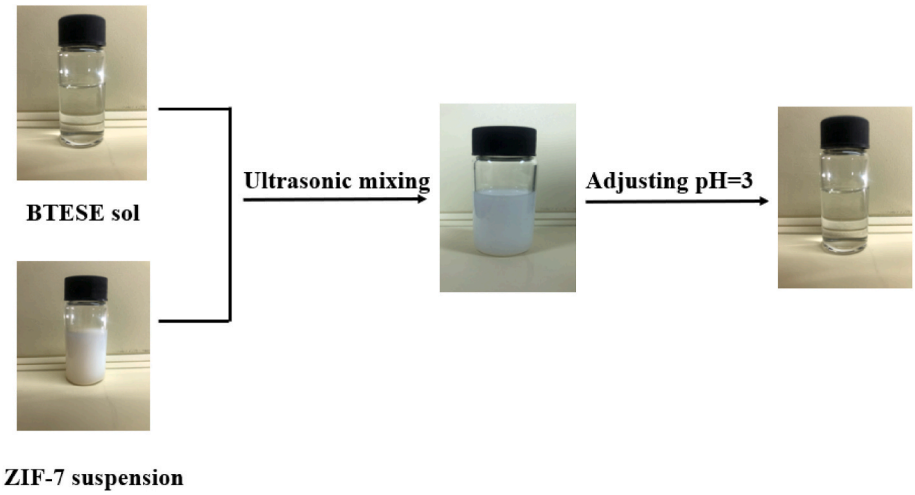

Fig. 2. Flow diagram for the synthesis of ZIF-7/BTESE sols.

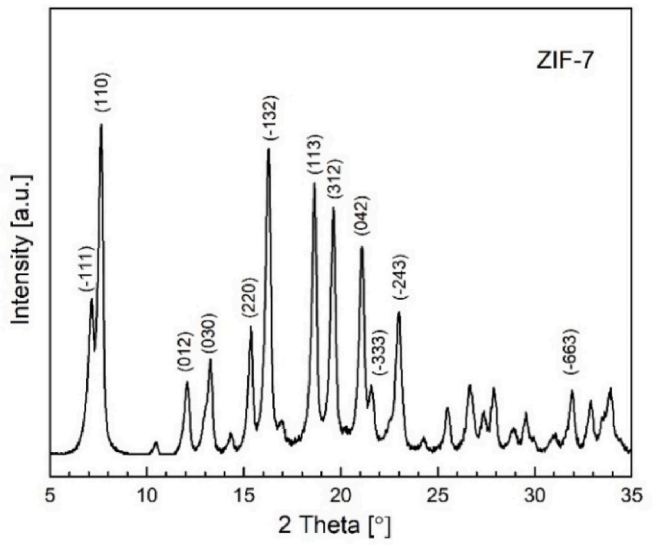

Fig. 3. XRD pattern of ZIF-7 nanoparticles.

nm might be appropriate to obtain stable as well as homogeneous dispersed sols.

The solvent in the synthesis of BTESE sol is ethanol. Therefore, the uniform dispersion of ZIF-7 nanoparticles in ethanol solvent is a key step in determining whether ZIF-7 nanoparticles can be incorporated into BTESE sol. The ultrasonic dispersion technology was used to disperse ZIF-7 in ethanol solvent and particle size distribution is shown in Fig. 5. It can be seen that ZIF-7 nanoparticles dispersed in ethanol solution have uniform size around 68 nm.

During the preparation process of the BTESE membrane, a heat treatment process of 400 °C is required, as this treatment process is directly related to the interface area between ZIF-7 and polyamide matrix. Hence, to prepare a ZIF-7/BTESE membrane with stable

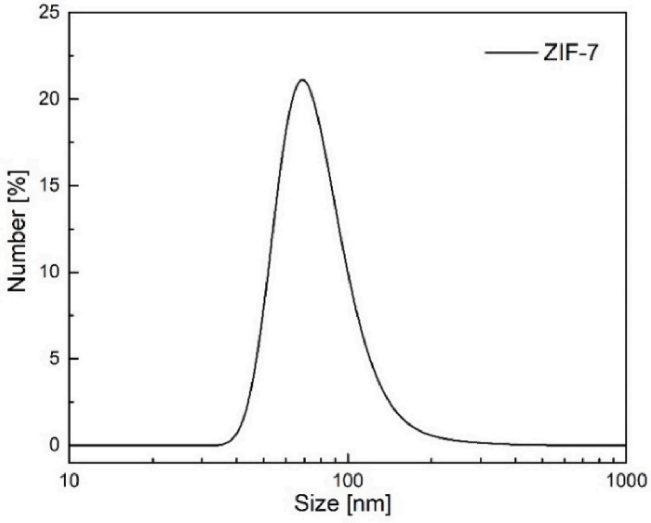

Fig. 5. Particle size distribution of ZIF-7 suspension after ultrasonic treatment.

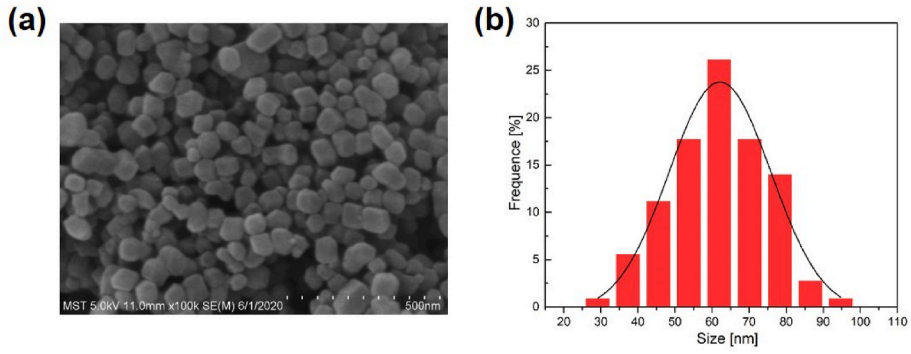

Fig. 4. (a) SEM image and (b) size distribution of ZIF-7 nanoparticles.

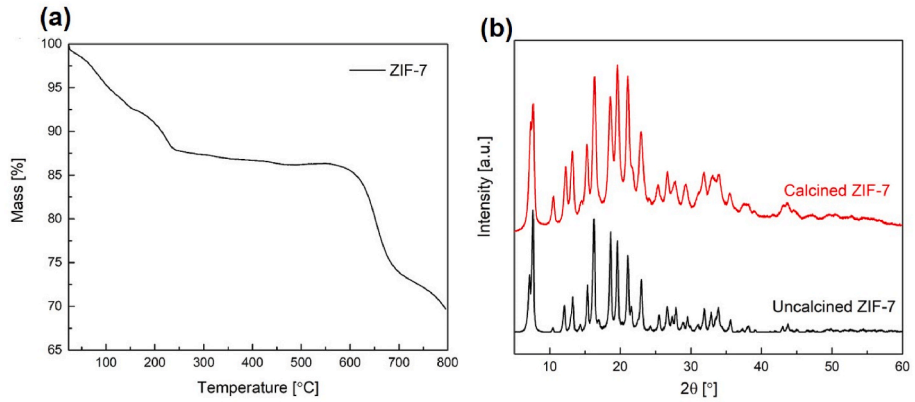

Fig. 6. (a) TGA curve of ZIF-7 nanoparticles (b) XRD patterns of freshly prepared ZIF-7 powder and ZIF-7 nanoparticles after calcination at 400 °C.

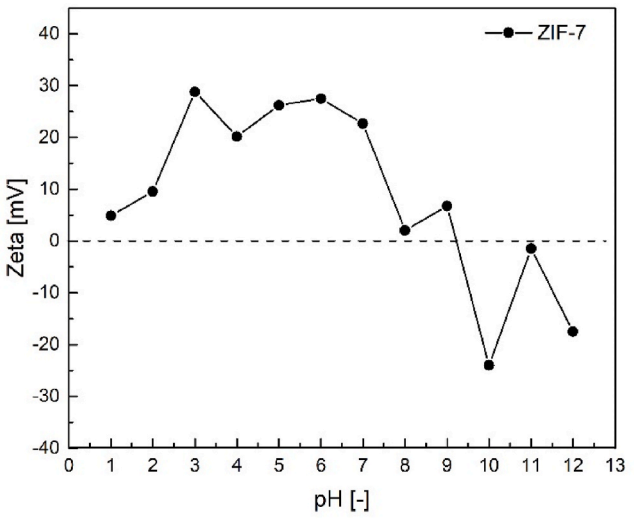

Fig. 7. The Zeta potential of ZIF-7 nanoparticles as a function of pH.

structure, the thermal stability of the ZIF-7 nanoparticles has been proposed to be of great importance. The thermogravimetric curve of ZIF-7 nanoparticles under nitrogen atmosphere and the XRD spectrum after calcination at 400 °C was investigated by using TGA and XRD. It can be seen from Fig. 6(a) that ZIF-7 has very good thermal stability and does not begin to decompose until temperature reaches approximately 560 °C [28]. In addition, it should be noted in Fig. 6(b) that the XRD spectrum of the ZIF-7 nanoparticles after calcination at 400 °C is consistent with the spectrum of the particles before calcination, indicating that the form of ZIF-7 nanoparticles remains unchanged after calcination at 400 °C, which proves its excellent thermal stability.

When the nanoparticles are dispersed in the solvent, Zeta potential has a great relationship with the pH of solvent. The electrostatic repulsion between the particles is proportional to the absolute value of the Zeta potential. Thus, the dispersion of nanoparticles in the solvent becomes better as the absolute value of the Zeta potential increases. Fig. 7 illustrates the relationship between Zeta potential of ZIF-7 and the solution pH. As the BTESE sols synthesis is only related to acid-catalyzed process, the Zeta potential of the ZIF-7 suspension under alkaline conditions is not considered. As shown in Fig. 7, the absolute value of the Zeta potential of ZIF-7 nanoparticles reaches a maximum at pH = 3. This means that adjusting the pH value to 3 might produce fairly desired dispersion.

Through the above characterization results of ZIF-7, the as-synthesized ZIF-7 can provide feasible conditions for the preparation of ZIF-7/BTESE membranes.

3.2. Particle size distributions of organosilica sols

The particle size distribution of organosilica sols is measured by using DLS. It is found that the particle size of BTESE sol presents a unimodal distribution, and its average particle size is 4 nm in Fig. 8. Along with the introduction of ZIF-7 into BTESE sol, the particle sizes of *E*-ZIF-7-0.05 and *E*-ZIF-7-0.1 sol show a bimodal distribution. The particle size is around 5 nm which can be attributed to BTESE sol, and the size of ZIF-7 nanoparticles is around 300 nm due to the aggregation between the particles. This result suggests that the introduction of ZIF-7 nanoparticles efficiently increases the average particle size of BTESE sol and the size of ZIF-7 particles, but decreases the size distribution intensity of BTESE sol. As the content of ZIF-7 comes up to n (ZIF-7): n (BTESE) = 0.2, the particle size distribution peak of the BTESE sol is barely visible. It can be explained that as the content of ZIF-7 increases, ZIF-7 particles might adhere to the BTESE, resulting in a corresponding increase in the particle size of the BTESE sol. When the BTESE network is completely attached to the ZIF-7, the particle size distribution peak of the BTESE sol disappears, forming the *E*-ZIF-7-0.2 sol with a unimodal distribution and a larger average particle size.

3.3. Chemical composition analysis of ZIF-7/BTESE powders

Fig. 9 presents the XRD patterns of BTESE and ZIF-7/BTESE powders.

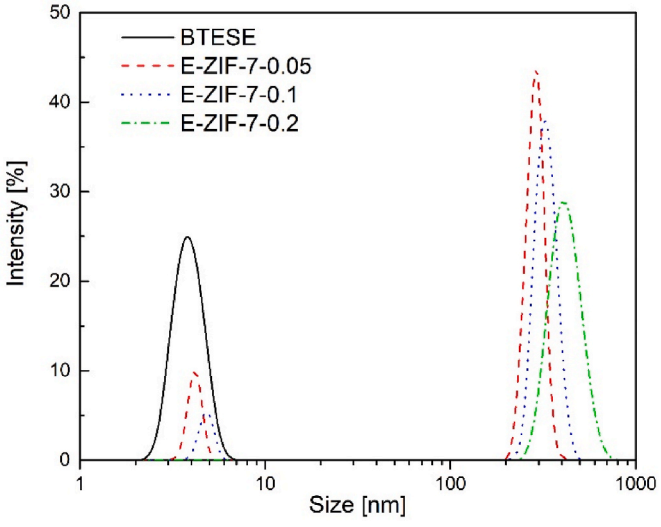

Fig. 8. Particle size distributions of BTESE and ZIF-7/BTESE sols.

The XRD spectrum of BTESE powder shows a broad diffraction peak in the range of 5–40°, indicating a disordered or amorphous structure in the BTESE powders [37]. The characteristic peaks of the ZIF-7 crystals in the ZIF-7/BTESE powder are not obvious, which may be because the characteristic peaks of the ZIF-7 crystals overlap with the diffraction peaks of the BTESE powder. Compared with the XRD spectra of BTESE powder, it can be found that with the increase of ZIF-7 content, the diffraction peak of ZIF-7/BTESE powder at about 20° is detected. This is probably due to the superposition effect of the strong diffraction peak of ZIF-7 crystal near 20° and BTESE powder diffraction peak. Another reason why the characteristic peaks of ZIF-7 crystals in ZIF-7/BTESE powder are not obvious is due to the low content of ZIF-7. When n (ZIF-7): n (BTESE) = 0.2, the *E*-ZIF-7-0.2 sample shows faint characteristic peaks of ZIF-7 crystal near 10 and 35°.

The surface and cross-sectional morphologies of the pure and ZIF-doped organosilica membranes were analyzed by SEM and the results are depicted in Fig. 10.

In Fig. 10 (a)–(d), the surface of the BTESE and ZIF-7/BTESE membranes are smooth without obvious cracks, indicating that the as-prepared membranes are integral. The white particles are randomly dispersed on the surface of the membrane, which may be ZIF-7 particles. The EDS analysis was conducted on the ZIF-7/BTESE membranes surface to understand the elemental distribution of the ZIF-doped organosilica membranes in Fig. S1 (a)–(c). The results demonstrate that the surface of the membranes have zinc element, indicating that ZIF-7 was successfully introduced. In addition, as the content of ZIF-7 increases, the content of zinc also increases accordingly. It can be seen from the cross-sectional SEM image in Fig. 10 (e) that the *E*-ZIF-7-0.2 membrane has an asymmetric structure including a α-Al_2O_3 support, a γ-Al_2O_3 intermedia layer and a top layer. The ZIF-7/BTESE membrane exhibited an ultrathin separation layer with the thickness of about 150 nm.

The particle dispersion of ZIF-7 in the organosilica was investigated by using a transmission electron microscope (TEM) and Fig. 11 displays the morphology of ZIF-7/BTESE powders precipitated in ethanol. It can be seen from Fig. 11 (d) that the black particles in the TEM photos have apparent lattice fringes, which manifests that the black particles are ZIF-7 [38]. Fig. 11(a–c) shows TEM photos of *E*-ZIF-7-0.05, *E*-ZIF-7-0.1 and *E*-ZIF-7-0.2 powders. As shown in the figure, the ZIF-7 particles are uniformly dispersed into the BTESE network structure at random. As the content of ZIF-7 increases, the distribution density of ZIF-7 particles in the BTESE network gradually increases. There is no significant change in the size of the ZIF-7 particles, and the nanoparticle size is about 10 nm. In comparison to the particle size (~60 nm) in the ZIF-7 suspension, the particle size of ZIF-7 becomes smaller after being incorporated into the BTESE network. The possible reason is that, after ZIF-7 was added into the BTESE network, and the subsequent heat treatment, the larger ZIF-7 crystal was decomposed into smaller ZIF-7 crystals, and the BTESE network structure formed a certain steric hindrance, preventing the aggregation of ZIF-7 crystals. The above results show that the ZIF-7 crystals are evenly dispersed into organosilica networks.

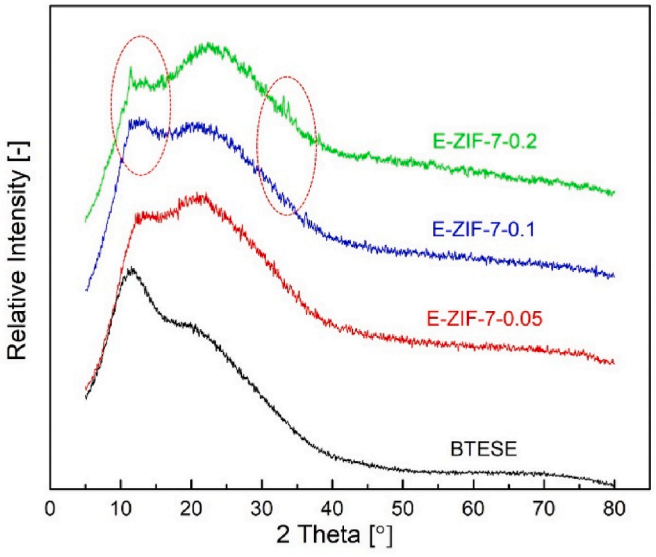

Fig. 9. XRD patterns of BTESE and ZIF-7/BTESE powders.

Fig. 12 is the FTIR spectra of BTESE and ZIF-7/BTESE powders in the range of 600–4000 cm^{-1} and the inset is the molecular structure of ZIF-7. Characteristic peaks located at ~3450 cm^{-1} and ~1628 cm^{-1} could be assigned to the stretching vibrations of Si–OH and H–O deformation vibration, respectively. The peak at ~1045 cm^{-1} can be attributed to the asymmetric stretching vibrations of *Si–O–*Si [33,39,40]. Compared with the FTIR spectra of BTESE powder, there are new chemical bonds in ZIF-7/BTESE powder at 1506 and 743 cm^{-1}, corresponding to the C═C and C–H bonds on the benzene ring in the ZIF-7 structure [35]. It is shown that as the content of ZIF-7 in derived polymeric powder increases, the peaks of the C═C and C–H bonds gradually become stronger. This result confirms that ZIF-7 is successfully introduced into the BTESE network structure.

XPS analysis was carried out to get a better understanding of the varieties of the chemical composition of ZIF-7/BTESE powder. The chemical elements in the powder structure of ZIF-7, BTESE and ZIF-7/BTESE were quantitatively analyzed by XPS characterization, and the results are shown in Fig. 13. The XPS full spectra of BTESE and ZIF-7 powders show the characteristic peaks of Si 2p and Zn 2p, respectively, while the ZIF-7/BTESE powder shows both Si 2p and Zn 2p characteristic peaks. It is obvious that as the content of ZIF-7 increases, the characteristic peak intensity of Zn 2p in the XPS spectrum of ZIF-7/BTESE powder gradually increases. Table 1 also summarizes the atomic ratio of ZIF-7/BTESE powder with different ZIF-7 content. The above results of TEM and FTIR show that ZIF-7 nanoparticles have been successfully introduced into the BTESE networks. Moreover, the proportion of ZIF-7 nanoparticles in the BTESE networks become larger along with an increase in ZIF-7 content.

3.4. Gas separation performance of nano-composite membranes

Gas permeance was measured with six single gases at a test temperature of 200 °C. Fig. S2 shows that as the measured gas molecular dynamic diameter increases, the gas permeance of BTESE and ZIF-7/BTESE membrane displays a downward trend. Additionally, BTESE membrane exhibits the highest gas permeance performance and when ZIF-7 was introduced into the BTESE networks, the gas permeance of the ZIF-7/BTESE membrane began to decline. However, with the introduction of ZIF-7, the extra-introduced free volume provides more sub-nano channels for gas transportation, thus the H_2 permeance of the resulting membranes gradually increases [24]. Meanwhile, though the mean free volume size becomes slightly larger, the rigidified chains may amplify the molecular sieve effect and result in an undiminished or even enhanced selectivity [28]. The gas permeance of *E*-ZIF-7-0.2 membrane shows a more prominent molecular sieving effect. The specific phenomenon is that the gas permeance of *E*-ZIF-7-0.2 membrane to CO_2, N_2, CH_4 and SF_6 drops sharply while the gas permeance of small molecules such as He and H_2 increases slowly. What is shown in Fig. S2(b) is that the permselectivity of H_2/CO_2 and H_2/N_2 of BTESE membrane is only 5.68 and 8. When the content of ZIF-7 ranges from n (ZIF-7): n (BTESE) = 0.05 to n (ZIF-7): n (BTESE) = 0.2, the permselectivity of H_2/CO_2 and H_2/N_2 of the ZIF-7/BTESE membrane increases from 8.78 and 11.8 to 22.7 and 159, respectively. The H_2/CO_2 and H_2/N_2 selectivity of ZIF-7/BTESE membrane grows rapidly when the content of ZIF-7 increases from n (ZIF-7): n (BTESE) = 0.1 to n (ZIF-7): n (BTESE) = 0.2. Compared with BTESE membrane, the permselectivity of H_2/CO_2 and H_2/N_2 of *E*-ZIF-7-0.2 membrane shows 4-fold and 20-fold increases, while its H_2 permeance maintains at 8.0×10^{-7} mol m^{-2} s^{-1}·Pa^{-1}.

Based on the analyses of TEM, FTIR and XPS results, Fig. S3 shows

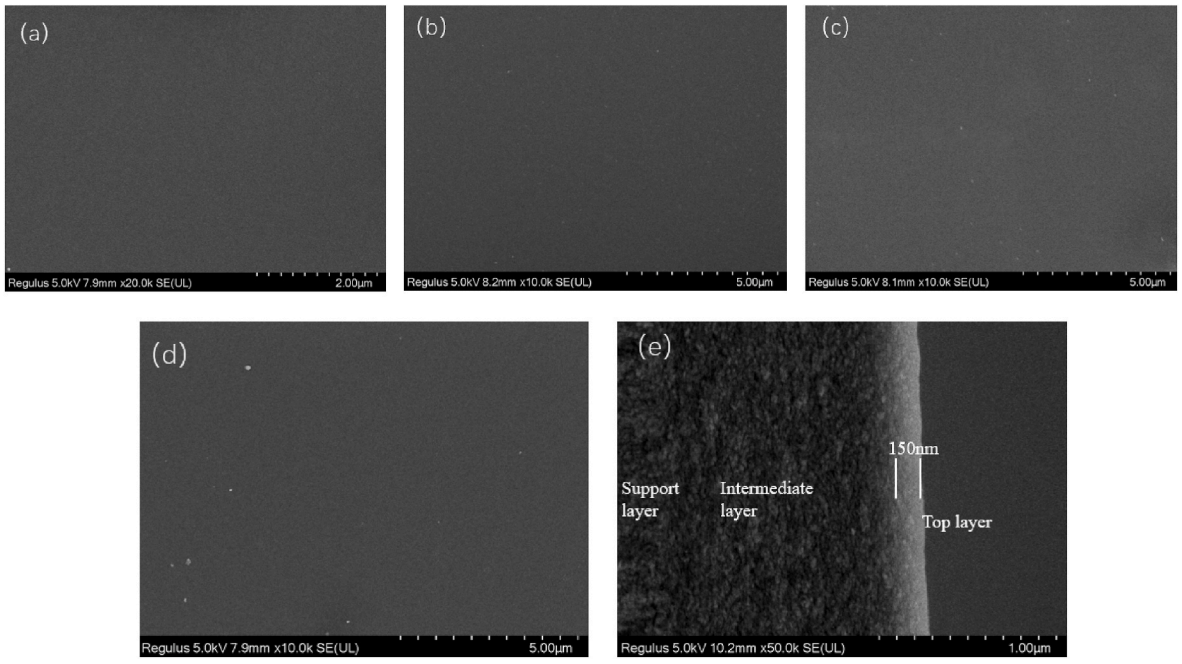

Fig. 10. Surface SEM images of (a) BTESE membrane, (b) *E*-ZIF-7-0.05 membrane, (c) *E*-ZIF-7-0.1 membrane, (d) *E*-ZIF-7-0.2 membrane, (e) cross-sectional SEM image of *E*-ZIF-7-0.2 membrane.

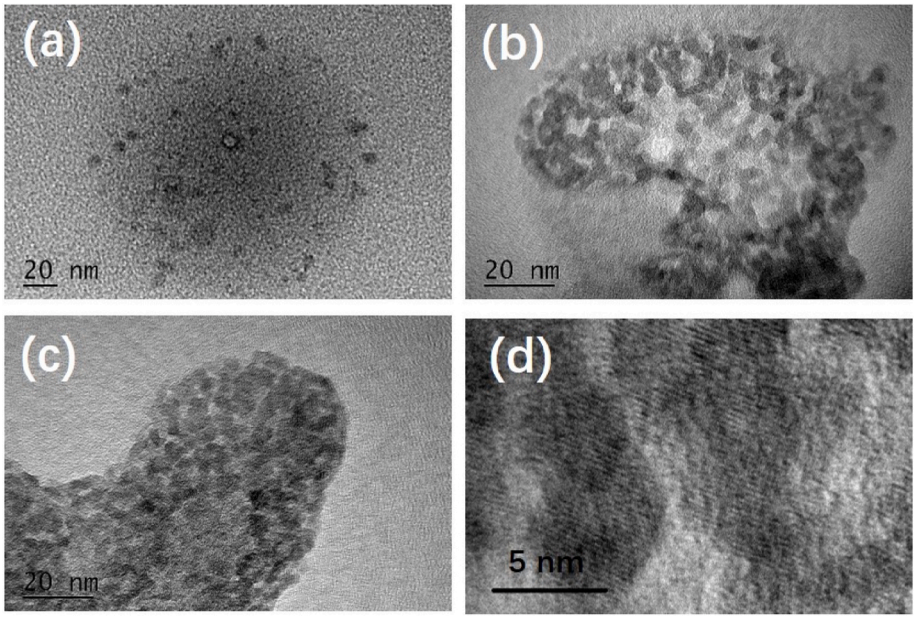

Fig. 11. TEM images of (a) *E*-ZIF-7-0.05, (b) *E*-ZIF-7-0.1 and (c, d) *E*-ZIF-7-0.2 powders.

the structure conjecture of ZIF-7/BTESE membrane for H_2/CO_2 separation. ZIF-7 nanoparticles are randomly distributed in the BTESE network. As the number of molar ratio rises, the distribution density of ZIF-7 nanoparticles also increases. Since the pore size of ZIF-7 is only 0.3 nm, gases with large size, such as CO_2 (dynamic diameter 0.33 nm) and N_2 (dynamic diameter 0.364 nm) with a larger molecular dynamic diameter cannot pass through ZIF-7 nanoparticles. Thereafter, ZIF-7 is introduced into the BTESE network, which prevents gases with large size from passing through the ZIF-7/BTESE membrane, while H_2, gas with small size (dynamic diameter 0.28 nm), can directly pass through ZIF-7 particles. As shown in the figure, when CO_2 passes through the ZIF-7/BTESE membrane, the permeation path will increase due to the blocking of ZIF-7, and the macroscopic phenomenon is manifested as a decrease in gas permeance. When the ratio of ZIF-7 in ZIF-7/BTESE membrane increases, it will obviously increase the permeation path of CO_2. Since the kinetic diameter of H_2 is smaller than the pore size of ZIF-7, ZIF-7 has a smaller permeation barrier to H_2. The conjecture diagram of the structure of the ZIF-7/BTESE membrane, as shown in Fig. S3, explains the influence of the introduction of the above-mentioned ZIF-7 on the gas permeance of the BTESE membrane. It can be concluded that the higher content of ZIF-7 will yield a longer permeation path for gases with large size through ZIF-7/BTESE membrane. The macroscopic phenomenon is that as the content of ZIF-7 increases, the selectivity of H_2/CO_2 and H_2/N_2 of the ZIF-7/BTESE membrane is greatly improved, while the H_2 permeance gradually increases.

To further understand the transport mechanism of six single gases

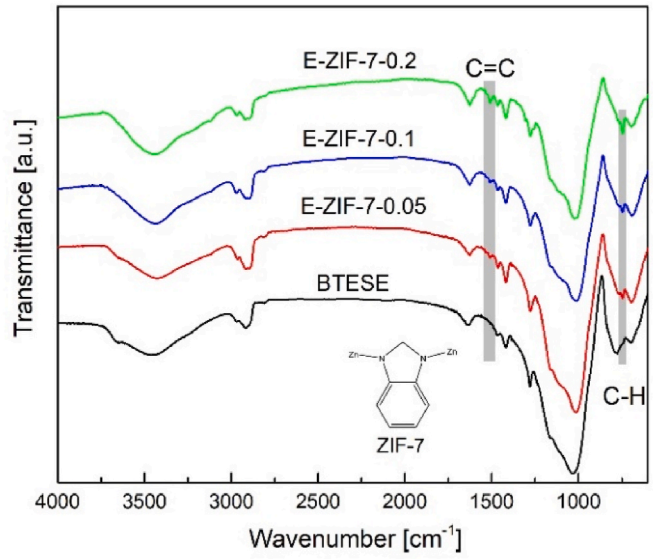

Fig. 12. FTIR spectra of BTESE and ZIF-7/BTESE powders.

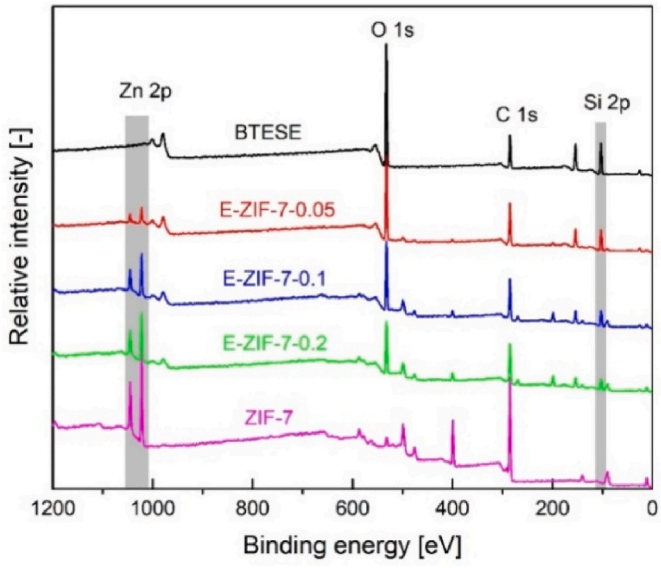

Fig. 13. XPS spectra of ZIF-7, BTESE and ZIF-7/BTESE powders.

Table 1
Atomic ratios of BTESE and ZIF-7/BTESE powders.

Sample	Si/%	C/%	O/%	Zn/%
BTESE	23.5	30.7	45.8	0
E-ZIF-7-0.05	20.8	41.5	35.9	1.8
E-ZIF-7-0.1	16.8	47.1	31	5.1
E-ZIF-7-0.2	14.6	51.8	27	6.6

through the ZIF-7/BTESE membranes, the relationship between gas permeance and temperature was investigated. The gas permeance of the ZIF-7/BTESE membranes can be calculated as follows:

$$F = F_0 \exp(\frac{-\Delta E}{RT}) \quad (3)$$

$$lnF = -\frac{\Delta E}{RT} + lnF_0 \quad (4)$$

In Equations (3) and (4), F, F_0, R, T, and ΔE are the gas permeance ($mol \cdot m^{-2}\ s^{-1}\ Pa^{-1}$), temperature independent parameter, gas constant ($J \cdot mol^{-1}\ K^{-1}$), absolute permeation temperature (K) and apparent activation energy ($J \cdot mol^{-1}$), respectively. The values of ΔE represent different gas diffusion mechanisms. In more details, positive ΔE indicates that the gas permeates through a membrane by activated diffusion, while the negative ΔE manifests the process is based on surface diffusion [41,42]. It can be seen from Fig. 14(a) that as the test temperature rises from 50 to 200 °C, the permeances of He, H_2, CO_2, N_2 and CH_4 all gradually increase, while the permeance of SF_6 gradually decreases. The slope of the fitted line for He, H_2, CO_2, N_2 and CH_4 is negative, whereas the slope of the fitted line for SF_6 is positive as shown in Fig. 14(b). According to formula (4), the activation energies of He, H_2, CO_2, N_2 and CH_4 are positive, indicating that their mass transfer mechanism through the *E*-ZIF-7-0.2 membrane is the activated diffusion mechanism. The activation energy of SF_6 is negative, illustrating that its mass transfer mechanism through the *E*-ZIF-7-0.2 membrane is surface diffusion.

Fig. 15 shows the H_2/CO_2 separation performance comparison among ZIF-7/BTESE membranes prepared in this study, BTESE membrane, MOFs membranes reported in the literature (ZIF-7, ZIF-8, ZIF-9, ZIF-90 and CAU-1), SiO_2 membrane, molecular sieve membranes and mixed matrix membranes incorporation of ZIFs. The H_2 permeance and H_2/CO_2 selectivity of pure MOFs membranes are generally low, for the difficulty to obtain a complete and defect-free MOFs membrane [43,44]. Thus, the separation layer of the usually prepared pure MOFs membrane is thicker to reduce the formation of defects, and the result is the lower H_2 permeance. In the process of crystal growth and membrane formation of MOFs membrane, the crystal growth does not follow certain directions so that large gaps are easily formed between the MOF crystals, and this causes poor membrane selectivity. From Fig. 15 the performance of the ZIF-7/BTESE membrane fabricated in this work, compared to that of other H_2/CO_2 separation membranes, maintains better H_2 permeability and H_2/CO_2 selectivity (far above the upper bound 2008). It can be argued that it has competitive advantages in the field of H_2/CO_2 membrane separation.

4. Conclusions

In summary, organosilica blended with ZIF-7 on a home-made tubular γ-alumina support was successfully fabricated via dip-coating method. Different molar ratios of ZIF-7 to BTESE have been investigated in order to get excellent gas separation performance. By series of characterization, it could be convinced that membranes with uniform and well-dispersed ZIF-7 nanoparticles in the BTESE network have been fabricated. The composite membrane exhibited excellent selectivity, while maintaining high H_2 permeance. Moreover, it was found that with the doping content of ZIF-7 increased, H_2 permeance of ZIF-7/BTESE membranes remained basically unchanged, whereas the permeance of larger gases displayed a dramatically drop. The membrane, when the molar ratio of ZIF-7: BTESE = 0.2, showed the excellent H_2/CO_2 (22.7) and H_2/N_2 (159) selectivity, with a comparatively outstanding H_2 permeance at 8.0×10^{-7} mol $m^{-2}\ s^{-1} \cdot Pa^{-1}$.

CRediT authorship contribution statement

Die He: Writing – original draft, Methodology, Conceptualization, Data curation, Formal analysis, Investigation. **Hengfei Zhang:** Writing – review & editing, Methodology, Investigation, Formal analysis. **Yi Ren:** Investigation, Methodology, Writing – review & editing. **Hong Qi:** Writing – review & editing, Supervision, Resources, Investigation, Funding acquisition.

Declaration of competing interest

The authors declare that they have no known competing financial interests or personal relationships that could have appeared to influence

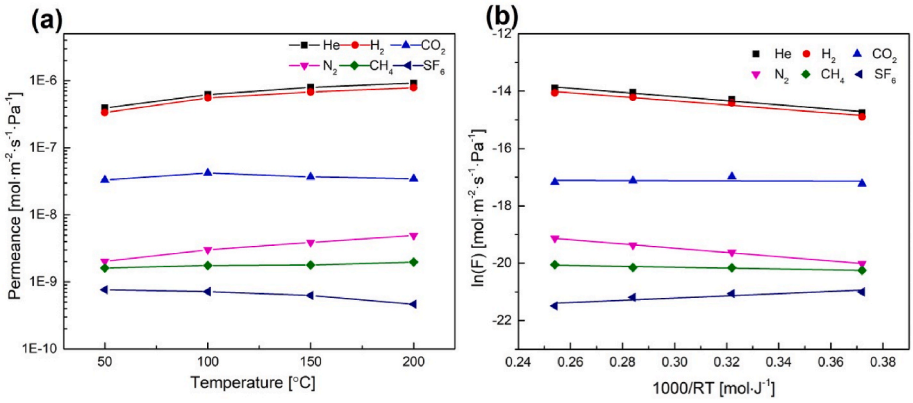

Fig. 14. (a) Temperature dependance of gas permeance (b) gas permeance calculated based on Arrhenius equation for *E*-ZIF-7-0.2 membrane.

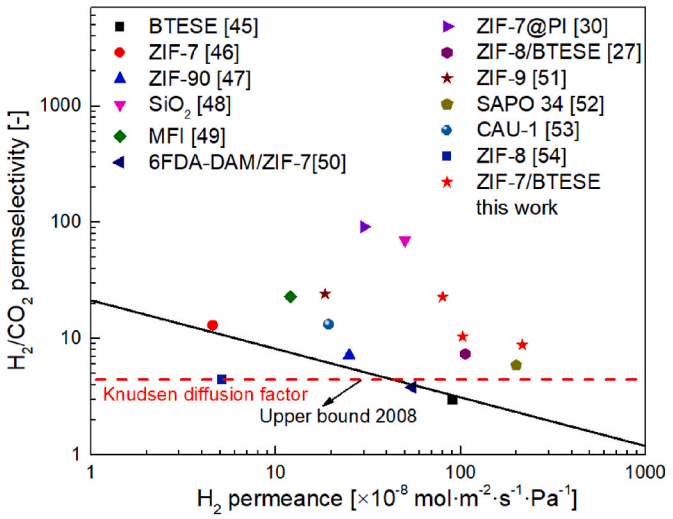

Fig. 15. Comparison of H_2/CO_2 separation performance for ZIF-7/BTESE membranes prepared in this study with literature data for other membranes [27,30,45–54].

the work reported in this paper.

Acknowledgments

This work is supported by the National Natural Science Foundation of China (21490581), China Petroleum & Chemical Corporation (317008-6) and Guangxi Innovation Driven Development Foundation (AA172204092).

Appendix A. Supplementary data

Supplementary data to this article can be found online at https://doi.org/10.1016/j.micromeso.2021.111674.

References

[1] W. Chen, C. Chen, Water gas shift reaction for hydrogen production and carbon dioxide capture: a review, Appl. Energy 258 (2020) 114078.
[2] A.Y. Ku, P. Kulkarni, R. Shisler, W. Wei, Membrane performance requirements for carbon dioxide capture using hydrogen-selective membranes in integrated gasification combined cycle (IGCC) power plants, J. Membr. Sci. 367 (2011) 233–239.
[3] J. Dong, Y.S. Lin, M. Kanezashi, Z. Tang, Microporous inorganic membranes for high temperature hydrogen purification, J. Appl. Phys. 104 (2008) 121301.
[4] P. Li, Z. Wang, Z. Qiao, Y. Liu, X. Cao, W. Li, J. Wang, S. Wang, Recent developments in membranes for efficient hydrogen purification, J. Membr. Sci. 495 (2015) 130–168.
[5] S. Japip, K. Liao, T. Chung, Molecularly tuned free volume of vapor cross-linked 6FDA-Durene/ZIF-71 MMMs for H_2/CO_2 separation at 150 °C, Adv. Mater. 29 (2017) 1603833.
[6] N. Sazali, M.A. Mohamed, W.N.W. Salleh, Membranes for hydrogen separation: a significant review, Int. J. Adv. Manuf. Technol. 107 (2020) 1859–1881.
[7] G.A. Neumann, J.F. Cavanaugh, X. Sun, E.M. Mazarico, D.E. Smith, M.T. Zuber, D. Mao, D.A. Paige, S.C. Solomon, C.M. Ernst, O.S. Barnouin, Bright and dark polar deposits on mercury: evidence for surface volatiles, Science 339 (2013) 296–300.
[8] S.P. Cardoso, I.S. Azenha, Z. Lin, I. Portugal, A.E. Rodrigues, C.M. Silva, Inorganic membranes for hydrogen separation, Separ. Purif. Rev. 47 (2018) 229–266.
[9] R. Xu, L. He, L. Li, M. Hou, Y. Wang, B. Zhang, C. Liang, T. Wang, Ultraselective carbon molecular sieve membrane for hydrogen purification, J. Energy Chem. 50 (2020) 16–24.
[10] F. Gallucci, E. Fernandez, P. Corengia, M. van Sint Annaland, Recent advances on membranes and membrane reactors for hydrogen production, Chem. Eng. Sci. 92 (2013) 40–66.
[11] L. Meng, T. Tsuru, Microporous membrane reactors for hydrogen production, Curr. Opin. Chem. Eng. 8 (2015) 83–88.
[12] J. Dong, Y.S. Lin, M. Kanezashi, Z. Tang, Microporous inorganic membranes for high temperature hydrogen purification, J. Appl. Phys. 104 (2008) 121301.
[13] Z.Y. Yeo, T.L. Chew, P.W. Zhu, A.R. Mohamed, S. Chai, Synthesis and performance of microporous inorganic membranes for CO_2 separation:A review, J. Porous Mater. 20 (2013) 1457–1475.
[14] Y. Zhou, Y. Zhang, J. Xue, R. Wang, Z. Yin, L. Ding, H. Wang, Graphene oxide-modified g-C_3N_4 nanosheet membranes for efficient hydrogen purification, Chem. Eng. J. 420 (2021) 129574.
[15] Y. Zhao, P. Liu, Y. Ying, K. Wei, D. Zhao, D. Liu, Heating-driven assembly of covalent organic framework nanosheets for gas separation, J. Membr. Sci. 632 (2021) 119326.
[16] X. Ren, M. Kanezashi, H. Nagasawa, R. Xu, J. Zhong, T. Tsuru, Ceramic-supported polyhedral oligomeric silsesquioxane−organosilica nanocomposite membrane for efficient gas separation, Ind. Eng. Chem. Res. 58 (2019) 21708–21716.
[17] Y. Cheng, Y. Ying, S. Japip, S. Jiang, T. Chung, S. Zhang, D. Zhao, Advanced porous materials in mixed matrix membranes, Adv. Mater. 30 (2018) 1802401.
[18] Y. Zhao, D. Zhao, C. Kong, F. Zhou, T. Jiang, L. Chen, Design of thin and tubular MOFs-polymer mixed matrix membranes for highly selective separation of H_2 and CO_2, Separ. Purif. Technol. 220 (2019) 197–205.
[19] W. Guan, Y. Dai, C. Dong, X. Yang, Y. Xi, Zeolite imidazolate framework (ZIF)-based mixed matrix membranes for CO_2 separation: a review, J. Appl. Polym. Sci. 137 (2020) 48968.
[20] S.S. Sankar, K. Karthick, K. Sangeetha, A. Karmakar, S. Kundu, Transition-metal-based zeolite imidazolate framework nanofibers via an electrospinning approach: a review, ACS Omega 5 (2020) 57–67.
[21] B. Zornoza, C. Tellez, J. Coronas, J. Gascon, F. Kapteijn, Metal organic framework based mixed matrix membranes: an increasingly important field of research with a large application potential, Microporous Mesoporous Mater. 166 (2013) 67–78.
[22] Q. Song, S.K. Nataraj, M.V. Roussenova, J.C. Tan, D.J. Hughes, W. Li, P. Bourgoin, M.A. Alam, A.K. Cheetham, S.A. Al-Muhtaseb, E. Sivaniah, Zeolitic imidazolate framework (ZIF-8) based polymer nanocomposite membranes for gas separation, Energy Environ. Sci. 5 (2012) 8359–8369.
[23] T. Li, Y. Pan, K. Peinemann, Z. Lai, Carbon dioxide selective mixed matrix composite membrane containing ZIF-7 nano-fillers, J. Membr. Sci. 425 (2013) 235–242.
[24] T. Yang, Y. Xiao, T. Chung, Poly-/metal-benzimidazole nano-composite membranes for hydrogen purification, Energy Environ. Sci. 4 (2011) 4171–4180.
[25] C. Kong, H. Du, L. Chen, B. Chen, Nanoscale MOF/organosilica membranes on tubular ceramic substrates for highly selective gas separation, Energy Environ. Sci. 10 (2017) 1812–1819.
[26] Y. Li, F. Liang, H. Bux, A. Feldhoff, W. Yang, J. Caro, Molecular sieve membrane: supported metal-organic framework with high hydrogen selectivity, Angew. Chem. Int. Ed. 49 (2010) 548–551.

[27] Y. Peng, Y. Li, Y. Ban, H. Jin, W. Jiao, X. Liu, W. Yang, Metal-organic framework nanosheets as building blocks for molecular sieving membranes, Science 346 (2014) 1356–1359.
[28] X. Ma, X. Wu, J. Caro, A. Huang, Polymer composite membrane with penetrating ZIF-7 sheets displays high hydrogen permselectivity, Angew. Chem. Int. Ed. 58 (2019) 16156–16160.
[29] Y. Peng, Y. Li, Y. Ban, W. Yang, Two-dimensional metal-organic framework nanosheets for membrane-based gas separation, Angew. Chem. Int. Ed. 56 (2017) 9757–9761.
[30] Y. Li, F. Liang, H. Bux, W. Yang, J. Caro, Zeolitic imidazolate framework ZIF-7 based molecular sieve membrane for hydrogen separation, J. Membr. Sci. 354 (2010) 48–54.
[31] Y. Ying, Y. Xiao, J. Ma, X. Guo, H. Huang, Q. Yang, D. Liu, C. Zhong, Recovery of acetone from aqueous solution by ZIF-7/PDMS mixed matrix membranes, RSC Adv. 5 (2015) 28394–28400.
[32] X. Huang, J. Zhang, X. Chen, $[Zn(bim)_2]\cdot(H_2O)_{1.67}$: a metal-organic open-framework with sodalite topology, Chin. Sci. Bull. 48 (2003) 1531–1534.
[33] H. Zhang, D. He, S. Niu, H. Qi, Tuning the microstructure of organosilica membranes with improved gas permselectivity via the co-polymerization of 1,2-bis (triethoxysilyl) ethane and 1,2-bis(triethoxysilyl)methane, Int. J. Hydrogen Energy 46 (2021) 17221–17230.
[34] K.S. Park, Z. Ni, A.P. Côté, J.Y. Choi, R. Huang, F.J. Uribe-Romo, H.K. Chae, M. O'Keeffe, O.M. Yaghi, Exceptional chemical and thermal stability of zeolitic imidazolate frameworks, Proc. Natl. Acad. Sci. U.S.A. 103 (2006) 10186–10191.
[35] C. Kang, Y. Lin, Y. Huang, K. Tung, K. Chang, J. Chen, W. Hung, K. Lee, J. Lai, Synthesis of ZIF-7/chitosan mixed-matrix membranes with improved separation performance of water/ethanol mixtures, J. Membr. Sci. 438 (2013) 105–111.
[36] Y. Li, F. Liang, H. Bux, W. Yang, J. Caro, Zeolitic imidazolate framework ZIF-7 based molecular sieve membrane for hydrogen separation, J. Membr. Sci. 354 (2010) 48–54.
[37] H. Song, S. Zhao, J. Lei, C. Wang, H. Qi, Pd-doped organosilica membrane with enhanced gas permeability and hydrothermal stability for gas separation, J. Mater. Sci. 51 (2016) 6275–6286.
[38] Y. Li, H. Bux, A. Feldhoff, G. Li, W. Yang, J. Caro, Controllable synthesis of metal-organic frameworks: from MOF nanorods to oriented MOF membranes, Adv. Mater. 22 (2010) 3322–3326.
[39] P.H. Tchoua Ngamou, J.P. Overbeek, R. Kreiter, V.H.M. Veen, J.F. Vente, I. M. Wienk, P.F. Cuperus, M. Creatore, Plasma-deposited hybrid silica membranes with a controlled retention of organic bridges, J. Mater. Chem. A. 1 (2013) 5567–5576.
[40] R. Al-Oweini, H. El-Rassy, Synthesis and characterization by FTIR spectroscopy of silica aerogels prepared using several $Si(OR)_4$ and R " $Si(OR')_3$ precursors, J. Mol. Struct. 919 (2009) 140–145.
[41] T. Yoshioka, E. Nakanishi, T. Tsuru, M. Asaeda, Experimental studies of gas permeation through microporous silica membranes, AIChE J. 47 (2001) 2052–2063.
[42] H. Nagasawa, T. Niimi, M. Kanezashi, T. Yoshioka, T. Tsuru, Modified gas-translation model for prediction of gas permeation through microporous organosilica membranes, AIChE J. 60 (2014) 4199–4210.
[43] W. Li, Y. Zhang, Q. Li, G. Zhang, Metal−organic framework composite membranes: synthesis and separation applications, Chem. Eng. Sci. 135 (2015) 232–257.
[44] T.R. Cook, Y. Zheng, P.J. Stang, Metal-organic frameworks and self-assembled supramolecular coordination complexes: comparing and contrasting the design, synthesis, and functionality of metal-organic materials, Chem. Rev. 113 (2013) 734–777.
[45] N. Moriyama, H. Nagasawa, M. Kanezashi, K. Ito, T. Tsuru, Bis(triethoxysilyl) ethane (BTESE)-derived silica membranes: pore formation mechanism and gas permeation properties, J. Sol. Gel Sci. Technol. 86 (2018) 63–72.
[46] Y. Li, F. Liang, H. Bux, W. Yang, J. Caro, Zeolitic imidazolate framework ZIF-7 based molecular sieve membrane for hydrogen separation, J. Membr. Sci. 354 (2010) 48–54.
[47] A. Huang, W. Dou, J. Caro, Steam-stable zeolitic imidazolate framework ZIF-90 membrane with hydrogen selectivity through covalent functionalization, J. Am. Chem. Soc. 132 (2010) 15562–15564.
[48] R.M. de Vos, H. Verweij, High-selectivity, high-flux silica membranes for gas separation, Science 279 (1998) 1710–1711.
[49] H. Wang, X. Dong, Y.S. Lin, Highly stable bilayer MFI zeolite membranes for high temperature hydrogen separation, J. Membr. Sci. 450 (2014) 425–432.
[50] S. Park, K.Y. Cho, H.K. Jeong, Polyimide/ZIF-7 mixed-matrix membranes: understanding the in situ confined formation of the ZIF-7 phases inside a polymer and their effects on gas separations, J. Mater. Chem. A. 8 (2020) 11210–11217.
[51] J. Liu, C. Liu, A. Huang, Co-based zeolitic imidazolate framework ZIF-9 membranes prepared on α-Al_2O_3 tubes through covalent modification for hydrogen separation, Int. J. Hydrogen Energy 45 (2020) 703–711.
[52] J.K. Das, N. Das, S. Bandyopadhyay, Highly selective SAPO 34 membrane on surface modified clayealumina tubular support for H_2/CO_2 separation, Int. J. Hydrogen Energy 37 (2012) 10354–10364.
[53] S. Zhou, X. Zou, F. Sun, H. Ren, J. Liu, F. Zhang, N. Zhao, G. Zhu, Development of hydrogen-selective CAU-1 MOF membranes for hydrogen purification by 'dual-metal-source ' approach, Int. J. Hydrogen Energy 38 (2013) 5338–5347.
[54] H. Bux, F. Liang, Y. Li, J. Cravillon, M. Wiebcke, J. Caro, Zeolitic imidazolate framework membrane with molecular sieving properties by microwave-assisted solvothermal synthesis, J. Am. Chem. Soc. 131 (2009) 16000–16001.